SLAC–PUB–7547
November 1997

Possibility to measure the Poincaré section map of a circular accelerator*

Chun-xi Wang and John Irwin
Stanford Linear Accelerator Center, Stanford University, Stanford, CA 94309

Abstract

Nonlinear beam dynamics is an important issue in accelerator systems. The Poincaré section map plays a basic role in characterizing and analyzing such a nonlinear system. Although many kinds of nonlinear beam dynamics experiments have been conducted, no direct measurement of a nonlinear map has been reported for an accelerator in normal operation mode. In this paper, we will show that it appears possible to measure the Poincaré section map of a circular accelerator to a surprisingly high order and accuracy based on present technology. Such measurements could significantly advance our understanding of the beam dynamics in an accelerator.

Submitted to Physical Review E

*Work supported by Department of Energy contract DE–AC03–76SF00515.

1 Introduction

It is well known that the beam dynamics in accelerator systems is intrinsically nonlinear. In circular accelerators nonlinearity is one of the major factors that limits stability and influences dynamics of halos. In this paper, we focus on the beam dynamics issues in electron storage rings. In addition to the large effort invested into the design of an accelerator to control nonlinearities, it is essential to determine nonlinearities in the "as-built" machine in order to understand and improve its performance. A standard way to characterize the single particle beam dynamics in a periodic system is via the Poincaré section map $\mathcal{M}$ in phase space. For any initial phase space point X^i, the map $\mathcal{M}$ gives the new phase space vector X^f after one turn.

$$\mathcal{M} : X^i \to X^f \tag{1}$$

There are many ways to represent a map $\mathcal{M}$. In this paper, we use the map representation in terms of Taylor series:

$$X_k^f = X_k^0 + R_{kl}X_l^i + T_{klm}X_l^iX_m^i + U_{klmp}X_l^iX_m^iX_p^i + V_{klmpq}X_l^iX_m^iX_p^iX_q^i + \cdots \tag{2}$$

where the summation convention on the repeated indices is assumed. X_k is the k-th component of a phase space vector. If the closed orbit is chosen as the coordinate origin, $X_k^0 = 0$. Determination of the map is equivalent to the determination of the coefficients X^0, R, T, U, etc.

There are many kinds of single particle beam dynamics experiments, which roughly fall into two categories. One is lattice-diagnostic oriented. In this case, the accelerator is in a normal operation condition and the nonlinearity is weak. Only the linear transfer matrix R and its relation to the designed lattice and various errors in the system are pursued.[1, 2] No successful measurements of high order coefficients have been reported[†] , although some nonlinear quantities such as tune-shift-with-amplitude coefficients have been measured.[3] The other kind of experiment is to study the nonlinear beam dynamics by introducing significant nonlinear perturbations into the system via external fields or driving the beam to certain nonlinear resonances.[4, 5, 6] In such cases, the nonlinear effects are significantly enhanced or even dominate the beam motion. Although such experiments are interesting, they provide limited information on the dynamics of an accelerator in its normal operation mode.

In this paper, we will show that it appears possible to measure the Poincaré section map of a normal operation machine to a surprisingly high order and accuracy using presently available high resolution beam position monitors. There are many issues concerning the map measurement. They can be grouped as:

1. physical effects influencing the one-turn map,
   - single-particle map vs. beam-centroid map (3)
   - wake field effects (4)

[†]M. Lee informed us of his unsuccessful attempt to fit some 2-nd order coefficients at SPEAR.

- radiation damping and quantum excitation (5)
- stability of the map in the presence of power supply ripples, temperature fluctuations, ground motion, etc. (5)

2. measurement of the map (2),
   - number of data pairs to be measured and time required to collect data (2)
   - number of kickers required to explore the complete phase space (2)
   - number of turns that can be used for data collection after kicks (2,3,4)
   - effect of BPM resolution and nonlinearity (7)
   - beam energy resolution and control of beam energy (2,7)
3. extraction of map coefficients by fitting (2), and
   - extracting the single-particle map from the beam-centroid map (3)
   - map order to be used and convergence of fitting (6)
   - error estimate and hypothesis test (8)
   - advantages and drawbacks to break down the dimension of fitting (8)
4. error reduction in map extraction (9).
   - role of symplecticity (9)
   - numeric errors and condition of the design matrix (9)
   - using orthogonal series (9)
   - optimal ways to sample phase space (9)

Numbers in the brackets indicate the section in which the topic is addressed. We will first describe how to implement the experiment and reasons behind it, then address key issues that may affect such experiments. Simulation results will be presented. The last group of items are related to better map fitting methods. Many questions remain open, but are not essential to this paper, and will not be discussed in detail.

2 Experiment implementation and map extraction method

The map $\mathcal{M}$ can be specified by a data set consisting of vector pairs $\{X^i,\ X^f\}$ which are the initial and final phase space positions. X^i must cover the phase space region of interest. In the approximate Taylor map representation, $\mathcal{M}$ is parameterized by its power series coefficients. We can measure the map as data pairs and then convert them into a Taylor representation by fitting. The reason we choose to work with the Taylor map is that the fitting problem is linear, although there is a well known drawback that the Taylor map is not necessarily symplectic in general and requires significantly more parameters than necessary.

Also, as will be addressed later, we actually measure the beam-centroid map, which may not be symplectic in general.

The measurement is straightforward, which requires a large number (at least not less than the number of parameters to be determined) of data pairs of sufficient accuracy (to be addressed later). They can be collected in many ways. In the following, we describe a general approach to illustrate the major considerations. For a particular ring, one may need to work around some instrument limitations by taking advantage of certain unique features of the ring.

To sample a certain phase space volume, fast kickers are required to kick the beam to various positions in phase space. After the beam is kicked, its turn-by-turn phase space positions are recorded. Due to the beam decoherence etc. discussed later, a limited number of turns may be used after each kick. Before the next kick to sample other phase space points, the beam needs to be fully damped to the equilibrium orbit. This process can be repeated to obtain the required number of data pairs. In addition to tracking the beam centroid motion, we need to know the equilibrium emittances and energy spread in order to correct for the difference between the beam-centroid map and the single-particle map. See section 3 for details.

Due to the short damping time in an electron machine, thousands of data pairs can be collected in one hour. For example, the PEP-II low energy ring's horizontal damping time is $\tau_x = 40$ ms. If one assumes measuring each data pair takes about $10\tau_x$ (i.e. only one turn is observed for each kick), 9000 data pairs can be collected within an hour. If 10 turn data after a kick can be used, 90,000 data pairs can be collected each hour. In practice, the data collection speed may be limited by the time for the kickers to recover, or reading data from BPM digitizers.

Ideally two kickers are required in each plane to sample both coordinate and momentum. However, one can use just one kicker and use many turns of data to sample various coordinates, provided that the beam decoherence is negligible during those turns. Generally, injection kickers can provide the necessary kicks in one and only one plane. To generate kicks in the other plane may require a new kicker in many rings. Special care is necessary to arrange the x and y kicks as well as the number of turns to be used. In some rings, it may be possible to sample the phase space by steering the inject beam. In such a case, one needs to evaluate whether the difference in the phase-space distribution of the injected bunches can yield significant errors due to decoherence. Moreover, the fluctuation of the injected currents may affect the accuracy of BPM readings.

Beam position monitors (BPMs) are standard devices to measure the beam's transverse position. Position and momentum can be determined with two BPMs assuming the nonlinearity between the BPMs is negligible. This assumption should be a very good approximation because the distance between neighboring BPMs is usually short compared to the circumference of the accelerator. Moreover, one can always choose a location where the nonlinearity is not likely to be a concern. To measure the full transverse phase space, two BPMs are required in each plane. The BPMs must be sufficiently fast to measure the turn-by-turn trajectory.

In order to study the energy dependency of a map, the beam energy can be changed by

varying the RF frequency of the accelerating field[7]. Instead of being measured individually, the relative energy changes can be deduced via

$$\frac{\Delta\omega_{RF}}{\omega_{RF}} = -(\frac{\Delta C}{C} - \frac{\Delta v}{v}) = -(\alpha_c - \frac{1}{\gamma^2})\delta + O(\delta^2) \tag{3}$$

where α_c is the linear momentum compaction factor of the ring and γ is the beam energy. Often a stored beam has undamped synchrotron oscillation due to noises in the RF system, etc. In case such energy variation is not negligible, the turn-by-turn beam energy has to be measured and taken into account in map fitting. We will discuss energy resolution in section 7.

The fitting procedure is the standard least-squares fitting, which will be illustrated via a 2D phase space $\{x, p\}$ example. The map to be fitted is

$$\begin{cases} x^f = x_0 + R_{11}x + R_{12}p + T_{111}x^2 + T_{112}xp + T_{122}p^2 + \cdots \\ p^f = p_0 + R_{21}x + R_{22}p + T_{211}x^2 + T_{212}xp + T_{222}p^2 + \cdots \end{cases} \tag{4}$$

Assume there are n terms in each series and a total of m data pairs $\{(x_i, p_i) \rightarrow (x_i^f, p_i^f),\ i = 1 \rightarrow m\}$. Then the x component of the map may be written as

$$\vec{x^f}_{m\times 1} = A_{m\times n} C_{n\times 1} \tag{5}$$

where

$$\vec{x^f} = [x_1^f, x_2^f, \cdots, x_m^f]\tilde{},$$

$$A = \begin{bmatrix} 1 & x_1 & p_1 & x_1^2 & x_1p_1 & p_1^2 & \cdots \\ 1 & x_2 & p_2 & x_2^2 & x_2p_2 & p_2^2 & \cdots \\ \cdot & \cdot & \cdot & \cdot & \cdot & \cdot & \cdot \\ \cdot & \cdot & \cdot & \cdot & \cdot & \cdot & \cdot \\ 1 & x_m & p_m & x_m^2 & x_mp_m & p_m^2 & \cdots \end{bmatrix},$$

$$C = [x_0, R_{11}, R_{12}, T_{111}, T_{112}, T_{122}, \cdots, \text{ n-th coefficient }]\tilde{}$$

Since the vector $\vec{x^f}$ and design matrix A are determined by the measured data, we have a set of linear equations for the map coefficients C. Because the data contain errors, which will be addressed later, it is better to have $m \gg n$ so that the equations are overdetermined and look for the solution $\hat{C}$ which makes the norm $\|\vec{x^f} - A\hat{C}\|$ minimum (This is just the least-squares fitting method if we use the Euclidean norm).[8, 9] The solution reads

$$\hat{C} = A^+\vec{x^f} = (\tilde{A}A)^{-1}\tilde{A}\,\vec{x^f} \tag{6}$$

where A^+ is the pseudo-inverse (Moore-Penrose inverse) of the rectangular matrix A and $\tilde{A}$ is the transpose of A. The second expression can be used in the case $\tilde{A}A$ is not singular, otherwise more involved but standard mathematical routines are required. The same procedure holds for the other map component, i.e. $\vec{p^f}$. More discussions on fitting and error estimates will be presented in the following sections.

A very nice feature in map measurement is that all the measurement errors of transverse phase space are limited to the four BPMs which are steadily improving in quality[10, 11]. The

accuracy of the kickers do not play a role in the experiment as long as they are sufficiently fast. This is because the kickers are used to kick the beam to the neighborhood of a phase space point, while the exact beam position is measured by the BPMs. However, besides BPM accuracy, there are many beam dynamics issues that may limit our ability to measure the single-particle map. We will address these issues carefully.

The analyses presented later are based on simulations which use the SLAC/PEP-II design parameters[12]. A 9-th order Taylor map of the low energy ring (LER ring) in dynamical variables (x, P_x, y, P_y, δ) is used to model the single particle dynamics. The map has been used in the stability studies of the ring. Higher order (> 9) terms have no significant effects on beam dynamic aperture. To simulate the experiment, a large set of data pairs sampling the 5D phase space are generated randomly (or in grids). In addition, random errors are added to simulate the BPM and energy resolutions. If not specified, the number of data pairs used for fitting studies is 10 times the number of coefficients to be fit (i.e. $m/n = 10$). For simplicity, all fittings are done in 5D phase space simultaneously. Fitting results presented in this paper are only for the x component of the map. Results for other components are similar and, have the same design matrix A.

3 Single-particle map vs. beam-centroid map

Although our goal is to measure the single-particle map, our signals are from a bunch of particles. This may cause two kinds of problems. One is of dynamical origin–the collective effects. The other is of kinematic origin–the decoherence problem, which will exist even though all the interactions among the particles are negligible. This is because the BPM measures the centroid motion of a beam while each particle in the beam may have significantly different motion. A well-known example is the decoherence of a kicked beam, in which the centroid motion can be damped to zero although each particle's motion has not yet been damped.[14, 15, 16]

Neglecting collective effects, every particle in a beam follows the same single-particle map. Therefore, the beam centroid $\bar{X}$ follows

$$\begin{aligned}
\bar{X}^f_k &= [X^0_k + \hat{T}_{klm}\langle\delta X^i_l \delta X^i_m\rangle + \hat{U}_{klmp}\langle\delta X^i_l \delta X^i_m \delta X^i_p\rangle + \hat{V}_{klmpq}\langle\delta X^i_l \delta X^i_m \delta X^i_p \delta X^i_q\rangle + \cdots] \\
&\quad + \bar{X}^i_l [R_{kl} + \hat{U}_{klmp}\langle\delta X^i_m \delta X^i_p\rangle + \hat{V}_{klmpq}\langle\delta X^i_m \delta X^i_p \delta X^i_q\rangle + \cdots] \\
&\quad + \bar{X}^i_l \bar{X}^i_m [T_{klm} + \hat{V}_{klmpq}\langle\delta X^i_p \delta X^i_q\rangle + \cdots] \\
&\quad + \bar{X}^i_l \bar{X}^i_m \bar{X}^i_p [U_{klmp} + \cdots] \\
&\quad + \bar{X}^i_l \bar{X}^i_m \bar{X}^i_p \bar{X}^i_q [V_{klmpq} + \cdots] \\
&\quad + \cdots \\
&\equiv \bar{X}^0_k + \bar{R}_{kl}\bar{X}^i_l + \bar{T}_{klm}\bar{X}^i_l \bar{X}^i_m + \bar{U}_{klmp}\bar{X}^i_l \bar{X}^i_m \bar{X}^i_p + \bar{V}_{klmpq}\bar{X}^i_l \bar{X}^i_m \bar{X}^i_p \bar{X}^i_q + \cdots
\end{aligned} \tag{7}$$

where $\langle\cdots\rangle$ means average over the beam phase space distribution of X^i (assumed symmetric) and $\delta X = X - \bar{X}$ is a particle's deviation from the centroid.[‡] The hatted coefficients

[‡]For Gaussian distribution with $\langle\delta X\rangle = 0$, it is well known that $\langle\delta X_p \delta X_q\rangle = \sigma^2_{pq} = \sigma_p \sigma_q \rho_{pq}$, where ρ_{pq} is

are related to the unhatted ones by constant factors $\prod_i \binom{n(i)}{m(i)}$, where $\binom{n}{m}$ is the binomial coefficient and, $n(i)$ and $m(i)$ are the number of i among the running indices in the coefficients and in the $\langle\cdots\rangle$ terms respectively.[§] Note that permutations of the running indices are assumed not to contribute in Eqs. (2) and (7). We see that the beam centroid does not follow the single-particle map. Extra terms appear and depend on the beam phase space distribution. The difference between the centroid map and single-particle map decreases with the beam emittance. The two maps are the same if the nonlinearity is negligible.

It is important to realize that, as long as the beam maintains the same distribution, the coefficients $\bar{X}^0$, $\bar{R}$, $\bar{T}$, $\bar{U}$, etc. are constant, i.e. the beam centroid follows a well-defined Taylor map also, although this centroid map is different from the single-particle map. This observation allows one to overcome the single particle vs. beam problem, but imposes a strong condition on the experiment: for each measurement the beam must have the same phase space distribution. In an electron storage ring, radiation damping can accomplish this condition, by damping the beam to the equilibrium state before each kick. We assume the kick moves the beam centroid but does not significantly change the distributions relative to the centroid. Therefore, we have the same (equilibrium) phase space distribution for each measurement. In proton machines, it may be more difficult to control the phase space distribution.

The centroid map is changing after the beam is kicked due to filamentation etc. of the phase space distribution, limiting the number of turns which can be used. However, it should be safe to assume that the centroid map will not change significantly in a few turns, because the tune spread due to tune shift with amplitude and chromaticity is usually very small. The decoherence problem could be minimized by kicking a well-damped beam and using just one-turn data. Depending on various conditions for a particular measurement, it may be possible to use many-turn data. For our PEP-II example, at least 20 turns may be used.

After the centroid map is determined, the single-particle map can be solved using the information on the equilibrium beam phase space distribution (Thus we need to know the equilibrium emittances and energy spread). Note that the 0-th order term may appear in the centroid map even though $X^0 = 0$, which means that the closed orbit observed with BPMs is different from the closed orbit of the single-particle map and a coordinate translation may be necessary to obtain the single-particle map. Another important issue is that the centroid map is not symplectic in general, even though the single-particle map always is. Therefore, one has to be careful when trying to use symplecticity in fitting.

Notice that the corrections to the nonlinear coefficients are due to the coefficients which are at least two orders higher, assuming symmetric distributions. Therefore, the corrections are normally small for a well damped beam, which makes it much easier to extract the single-particle map. Moreover, the leading low order terms tend to dominate the corrections—which is the reason that Table-1 shows approximate linear dependency on beam emittance and

---

the covariance matrix. And $\langle \delta X_p^n \rangle = \begin{cases} 0 & n \text{ odd} \\ (n-1)!!\sigma_p^n & n \text{ even} \end{cases}$

[§]It is not important to understand these factors. Nonetheless, here is an example to help. In 5D, the index i runs from 1 to 5. The term $\hat{U}_{1224}\langle \delta X_2^i \delta X_4^i \rangle$ in $\bar{X}_l^i \hat{U}_{1lmp}\langle \delta X^i{}_m \delta X_p^i \rangle$ of Eq.(7) should read:

$$\hat{U}_{1224}\langle \delta X_2^i \delta X_4^i \rangle = \binom{0}{0}\binom{2}{1}\binom{0}{0}\binom{1}{1}\binom{0}{0} U_{1224}\langle \delta X_2^i \delta X_4^i \rangle = 2U_{1224}\langle \delta X_2^i \delta X_4^i \rangle.$$

emitt.	δ spread	$\bar{x}^0$	orders						
in ϵ_0	in σ_δ	in μm	1-st	2-nd	3-rd	4-th	5-th	6-th	7-th
0	1	1.03	2.60	7.3	11.9	18.9	16.6	23.4	24.5
1	1	0.66	2.66	9.9	11.7	19.4	16.9	25.2	25.0
2	1	0.25	2.72	12.4	11.6	20.0	17.3	27.3	25.5
4	1	-0.60	2.78	17.3	11.1	20.7	17.7	30.9	26.0
9	1	-2.50	3.24	29.8	10.0	22.7	19.0	39.4	27.1
0	2	4.13	9.66	25.7	41.6	68.9	60.3	93.0	97.2

Table 1: Maximum absolute corrections ($\times 10^3$) of coefficients in centroid maps with increasing beam emittance and energy spread for the PEP-II low energy ring.

square of energy spread. Taking the PEP-II low energy ring as an example, the maximum corrections at each order are shown in Table-1. The first two columns indicate the emittance and energy spread used for the calculation. ϵ_0 and σ_δ stand for the design emittance and energy spread of the ring. An uncorrelated 5D Gaussian distribution is used. The 0-th order terms are in μm, while others are the maximum corrections in 10^{-3} (for 10σ normalized coefficients[¶]). These may be compared with typical fitting errors shown in Table-2.

From Table-1 we see that, the 0-th order terms are negligible although non-zero. The corrections are fairly small in linear terms but become significant in nonlinear terms. However, only a few terms such as δP_x, $\delta^2 x$, $\delta^3 P_x$, $\delta^4 x$, $\delta^2 P_x x^2$, etc. actually have such significant changes. The corrections are dominated by the beam energy spread and not sensitive to the emittance growth. Therefore, it should not be difficult to fulfill the requirement of having the same beam for each kick during the measurement. Also the beam emittance and energy spread need not to be known very accurately in order to get sufficiently good correction.

Before moving on to the next topic, we would like to point out that, compared to the technique of harmonic analysis of multi-turn data, the map measurement described here has the advantage of being free from problems due to beam decoherence.

4 Wake field effects

In addition to the dynamics described by the single-particle map, a particle in a beam experiences wake fields due to collective effects. To measure the map, such wake field effects must be limited or procedures developed to correct its effects during map extraction. The best method to reduce collective effects is to reduce the beam current. However BPM resolution may decrease also. Therefore, beam current will need to be optimized for the best map measurement.

To estimate the wake field effects, we calculate the kicks on the beam centroid when a Gaussian bunch passes one turn of the ring. Assuming the betatron and synchrotron motions

[¶]For convenience, we normalize all dynamical variables to their 10σ values of the beam distribution, so that all map coefficients become dimensionless and their values reflect the importance of the corresponding terms.

are uncoupled, the change of beam centroid due to wake force is given by[17, 18, 13]

$$\Delta\delta = \frac{\langle \bar{\vec{F}}_\parallel \rangle}{E} \qquad \text{and} \qquad \Delta\vec{p}_\perp = \frac{\langle \bar{\vec{F}}_\perp \rangle}{E} \tag{8}$$

where E is the beam energy; $\langle \cdots \rangle$ means average over the bunch distribution; the top$^-$means integrated longitudinally over the wake structure. The average longitudinal and transverse impacts on the centroid are:

$$\begin{aligned} \langle \bar{\vec{F}}_\parallel \rangle &= -\frac{1}{N} \sum_{m=0}^{\infty} |I_m|^2 \; k_l^{(m)} \\ \langle \bar{\vec{F}}_\perp \rangle &= \frac{1}{N} \sum_{m=0}^{\infty} m(\Re[I_{m-1} I_m^*]\hat{x} - \Im[I_{m-1} I_m^*]\hat{y}) \; k_\perp^{(m)} \end{aligned} \tag{9}$$

where N is the number of particles in the bunch, I_m is the m-th moment of a Gaussian beam given by

$$I_m = Ne \sum_{n=0}^{[\frac{m}{2}]} (2n-1)!! \binom{m}{2n} (x_c + i\, y_c)^{m-2n} (\sigma_x^2 - \sigma_y^2 + i\; 2\rho\sigma_x\sigma_y)^n. \tag{10}$$

where x_c and y_c are the beam centroid position, and ρ is the correlation coefficient of the x and y distributions. $k_l^{(m)}$ and $k_\perp^{(m)}$ in Eq. (9) are the energy loss factor and transverse kick factor respectively for the multipole mode m, which are defined by

$$\begin{aligned} k_l^{(m)} &\equiv \int_0^\infty \frac{d\omega}{\pi} \; |\tilde{\rho}_\parallel(\omega)|^2 \; \Re[Z_m^\parallel(\omega)] \\ k_\perp^{(m)} &\equiv -\int_0^\infty \frac{d\omega}{\pi} \; |\tilde{\rho}_\parallel(\omega)|^2 \; \Im[Z_m^\perp(\omega)] \end{aligned} \tag{11}$$

where $\tilde{\rho}_\parallel$ is the Fourier transform of the longitudinal bunch distribution and Z_m is the impedance of the ring. The loss factor and kick factor are usually available for the longitudinal monopole mode and transverse dipole mode, because they are the dominating modes for a near-axis beam. The following scaling[18] provides a useful estimates for higher modes.

$$Z_m^\parallel \sim \frac{2}{b^{2m}} Z_0^\parallel \qquad \text{and} \qquad Z_m^\perp \sim \frac{1}{b^{2m-2}} Z_1^\perp \tag{12}$$

where b is the pipe radius.

In map measurements, we are interested in large amplitude motions with $x_c \gg \sigma_x$ and $y_c \gg \sigma_y$. Therefore I_m is dominated by the $n = 0$ term $(x_c + i\, y_c)^m$, which means the bunch acts like a macro particle. With the impedance estimates in Eq.(12), we get

$$\Delta\delta \sim -\frac{Nr_e}{\gamma} k_l^{(0)} \left[1 + 2\sum_{m=1}^{\infty} (\frac{r_c}{b})^{2m}\right] = -\frac{Nr_e}{\gamma} \; k_l^{(0)} \; \frac{1 + (\frac{r_c}{b})^2}{1 - (\frac{r_c}{b})^2} \tag{13}$$

and

$$\Delta\vec{p}_\perp \sim \frac{Nr_e}{\gamma} k_\perp^{(1)} (x_c\hat{x} + y_c\hat{y}) \sum_{m=1}^{\infty} m(\frac{r_c}{b})^{2m-2} = \frac{Nr_e}{\gamma} k_\perp^{(1)} (x_c\hat{x} + y_c\hat{y}) \left[1 - (\frac{r_c}{b})^2\right]^{-2} \tag{14}$$

where r_e is electron's classical radius, γ is the beam energy. $k_l^{(0)}$ and $k_\perp^{(1)}$ are the loss factor and kick factor for the lowest multipole modes. Fig. 1 is a plot of the nonlinear factors in Eqs. (13) & (14). Note that, the high order contributions become significant when the beam is close to the pipe. For beam displacement within 50% of the pipe radius (i.e. $r_c = 0.5b$) is a comfortable range, and 80% should be the upper limit. The nonlinear factors in $\Delta\delta$ and $\Delta\vec{p}_\perp$ are about the same within this range. Eq.(14) can be viewed as a thin kick map. Normalizing the dynamical variables to 10σ, we get roughly the same map coefficient for all orders, which reads

$$k_w \equiv \frac{Nr_e}{\gamma} k_\perp^{(1)} \, (\frac{10\sigma_x}{10\sigma_p}) = \frac{Nr_e}{\gamma} k_\perp^1 \, \bar{\beta} \tag{15}$$

where $\bar{\beta}$ is the average beta value of the ring. k_w provides a convenient way to estimate the significance of the wake effects.

For PEP-II LER, the design wake has $k_\perp^{(1)} \simeq 200V/pC\,m$ in c.g.s. unit.[13] For a 3 GeV, 10^{10} electron bunch, and $\bar{\beta} \simeq 10m$, we get $k_w \simeq 10^{-3}$. As a nonlinear coefficient, it is negligible; but for the linear map, such a perturbation is larger than our expected linear coefficient resolution (see Table-3) in map extraction. Thus we should be able to see its effect on the linear map (e.g. linear tune-shift). But such small linear perturbations will not change significantly the nonlinear map coefficients due to its feed-up with nonlinear coefficients. For the longitudinal wake, $k_l^{(0)} \simeq 10V/pC$, hence the effect on the beam energy is negligible. Therefore, wake field effects on map measurement are tolerable for the LER. Nonetheless, in general, wake fields may be a physical factor limiting map measurements, and specially designed low-current-high-resolution BPMs may be necessary for some rings. In experiments, one can identify wake effects by making measurements at different beam currents.

Since the wake effects may be observable in map measurements, methods to extract such effects should be pursued. In general, the wake field effects can not be characterized by one-turn maps since the interaction depends on the beam phase-space distribution and the history of the beam trajectory, which are time dependent. However, in our map measurement the phase space distribution can be considered the same for each one-turn pair measurement, and there is almost no multi-pass wake effects when just one-turn data are used. Therefore it is reasonable to characterize the wake effects by one-turn kicks given above. In such a case, we can measure maps at different currents and extrapolate to zero current. Such corrections should significantly reduce wake problems. Although locally the wake force depends linearly on beam current, it may show up nonlinearly in a one-turn map because of a coupling with lattice nonlinearities. However, such coupling should be fairly small and the linear dependence on current is expected to dominate.

In summary, wake fields may limit map measurements. k_w of Eq.(15) and the energy loss of Eq.(13) can be used to estimate the significance of wake field effects. In case it is not negligible, linear extrapolation to zero current can help to extract wake effects. However, we only considered one-turn wake force. When the impedance of a ring is large, using multi-turn data may further complicate problems through long-range wake effects.

5 Radiation damping, quantum excitation, and external noise

Radiation damping and quantum excitation are well-known physical processes that affect single-particle dynamics. When a particle passes through horizontal bending magnets, energy is lost due to radiation, vertical action is conserved, and horizontal action is increased. However, when the particle makes up the energy loss in RF system, actions in both directions are damped.[20] The relative action change reads $\frac{\Delta A^2}{A^2} = 2\frac{\tau_0}{\tau_x}$, i.e. the betatron amplitude change is $\frac{\Delta A}{A} = \frac{\tau_0}{\tau_x}$, where τ_0 is the revolution period and τ_x the transverse damping time. This number is very small in general. Therefore, unless BPM resolution is better than $10\sigma_x\frac{\Delta A}{A}$ (assuming maximum kick is 10σ), radiation damping effect should be negligible. For the PEP-II LER, $\frac{\tau_0}{\tau_x} \simeq 10^{-4}$ and $\sigma_x \simeq 1\,mm$, which yields an orbit change of $1\,\mu m$. Since the radiation damping could be taken into account in the one-turn map calculation, it is in any case not a fundamental limit to map measurements.

Due to the quantum nature of the radiation process, the smooth radiation damping picture could be modified by quantum excitations. To estimate the probable magnitude of a betatron amplitude fluctuation in a turn, we use the fact that beam emittance is determined by the balance of radiation damping and quantum excitation. Thus the expected action growth in one turn is $\Delta A^2 = 2\frac{\tau_0}{\tau_x}\sigma_x^2$, which is equivalent to an rms amplitude fluctuation $\Delta A \simeq \frac{\tau_0}{\tau_x}\sigma_x$. This should not be a concern.

Up till now, we have discussed various physical factors concerning the existence of a detectable single-particle map. Practically we still need to consider the stability of such a map under external disturbances (e.g. power supply ripples, temperature variations, ground motion) over the period of measurement. The dominant noise spectrum due to power supply ripple consists of the power line frequency and its harmonics, which are in the range of 100 – 1000 Hz. They are too slow to affect the single-turn measurement, but sufficiently fast to perturb the map from sample to sample. Due to their weak amplitude, the major effect of such high frequency noise is tune modulation. We added random linear tune kicks in our simulation to study the effect of such tune perturbations on map measurement, and found that up to 10^{-3} tune fluctuation is tolerable for LER map measurements with 10 μm BPMs. A very rough estimate can also be done for power supply ripple effects by converting the map coefficient variations to beam energy error via the generic dependency on $\frac{B}{1+\delta}$ in Hamiltonians. This yields $\Delta\delta \propto \frac{\Delta B}{B} \propto \frac{\Delta I}{I}$, where B and I are the magnetic fields and driving currents. PEP-II power supplies are regulated to better than 10^{-4}. Taking into account the significant damping due to transmission lines and eddy currents in vacuum chambers[21], $\Delta\delta$ should be less than our required energy resolution. In general, power supply ripples are limited by design because they may cause emittance growth. In case they are untolerablely large, one needs to pursue methods[22] to suppress any tune modulation. In fact, the most serious high frequency noises will probably come from the RF system. Turn-by-turn beam energy measurement may help to take into account the energy variation due to noisy longitudinal beam motion. In case there is a coupling between synchrotron and betatron motions, noisy RF system could limit the possibility of measuring the one-turn map.

Unlike the high frequency perturbations, very low frequency disturbances may be problematic. Here we are talking about diurnal temperature change[23], ground motion due to moon tides[24], etc. whose effects has been identified both in colliders for particle physics and rings for synchrotron radiation sources. For example, SPEAR experienced several hundred μm closed orbit oscillations because of diurnal temperature variation. Such changes may be tolerable for the machine's operation since control and feedback systems can be used to adjust machine performance. However, during map measurements, no feedback should be used and the lattice should be left alone. Therefore such very low frequency disturbances could be a problem and should be avoided. Fortunately map measurements can be done in a relatively short period of time. So the underlying map could be sufficiently stable. In general, such disturbances are machine and site dependent. We will not discuss them further. In experiments, one should check the stability of an unperturbed beam to identify possible problems, and furthermore, one should check the stability of the map measurements themselves.

6 Convergence of map fitting

Although a Poincaré section map is a century old concept, its extensive use for long-term stability studies in accelerators is fairly recent. The obvious concern is whether we can obtain a sufficiently accurate one-turn map to predict particle behavior after thousands or millions of turns, especially in face of the well-known sensitivity to initial conditions of nonlinear systems. We will not look into this general question here. It suffices to point out the well-known fact: many numerical studies[25, 26] supports the assumption that a 9-th order Taylor map is adequate for the stability studies in an electron machine. In our LER ring example, a 9-th order Taylor map has been used to generate tracking data and compare with our numerical fits.

Now consider our map fitting problem. First we discuss to which order one should try to fit. A more theoretical statement of the problem is how to choose the correct hypothesis (which is crucial for any fitting problems) about the map. Since we know that the 9-th order is about the highest order which may have some effects on beam dynamics of interest, as a bottom line, we can try to use a 9-th order fit map. In fact, our simulation studies show that it is possible to work with a much lower order fit map and the fitted maps will converge to the correct one (the 9-th order tracked map) as the fit-map order increases. The convergence of the fitted maps is a criteria to guarantee that we obtain the correct map (see section 8 for more discussions).

Table-2 shows the results of fitting simulated data to maps of increasingly higher orders. No random errors have been added to the data pairs yet. Since there are hundreds of coefficients with magnitudes spanning several orders, we have not shown the fitting results for each coefficient. Instead the maximum fitting errors ($|C_i^{fit} - C_i^{exact}|$) are tabulated for different orders in rows and for different fit-map orders in columns. For reference, the maximum coefficients of the original map at various orders are also included in the last row. Since the coefficients are for dynamical variables normalized to 10σ, they are dimensionless. For dynamical aperture concerns, values less than 10^{-3} are not significant (This is why we

fit-map order	orders					
	1-st	2-nd	3-rd	4-th	5-th	6-th
1	1.7×10^{-2}					
2	1.5×10^{-2}	4.4×10^{-2}				
3	1.1×10^{-3}	4.6×10^{-2}	2.0×10^{-2}			
4	5.1×10^{-4}	2.7×10^{-3}	2.2×10^{-2}	2.6×10^{-2}		
5	1.2×10^{-4}	1.5×10^{-3}	3.4×10^{-3}	2.9×10^{-2}	2.4×10^{-2}	
6	5.5×10^{-5}	1.0×10^{-4}	2.2×10^{-3}	2.0×10^{-3}	2.4×10^{-2}	4.1×10^{-2}
max. coeff.	0.86	0.10	0.27	0.25	0.21	0.23

Table 2: Maximum absolute fitting error dependency on fit-map order. The tracked map was 9-th order.

present absolute fitting errors instead of relative errors.) because a particle must be lost within 10^3 turns without radiation damping, otherwise the growth will be damped.[27] We see that the fitting is consistently improving and converges to the original map as the fit-map order increases. It also shows that to get a map to a certain order correctly, the fit-map order had better be 2 orders higher than the coefficient order (though in general this may be map dependent). The important point is that a sufficiently high order map must be used in fitting, even though only low order terms are of interest.

Now we will address the second apparent concern. For a high order map, there are hundreds even thousands of coefficients. How is it possible (Does it make sense?[28]) to fit so many parameters? We have to admit that such a possibility is indeed somewhat surprising, but fortunately the answer is affirmative. At least the method works well to fit significant coefficients. Another question that is closely related to the convergence problem is the domain dependency. Here, we will not address this issue in detail. Generally speaking, the larger the phase space domain used, the higher map order is required. In case only low order map coefficients are of interest, one may not want to kick the beam to 10σ. However, one should be aware that small beam amplitudes will make BPM errors more significant. In experiments, it is necessary to optimize the map order and phase space domain to be used under given conditions: expected (the design) map, beam aperture, BPM resolution etc. In this paper, we choose 8σ of the transverse distribution and 4σ energy distribution in simulations. Usually, there is larger than 12σ clearance in accelerators.

7 Dependency on the BPM resolution and energy resolution

As we pointed out before, we are trying to determine the map via a large set of data pairs. Obviously the accuracy of these data pairs determines how well the map is defined and how well the data can be fit by a map. There are two concerns with BPMs. One is the linearity of the BPM. Since we are measuring small nonlinear effects, the BPM itself

BPM res. in μm	orders				
	1-st	2-nd	3-rd	4-th	5-th
100	5.3×10^{-3}	4.4×10^{-3}	1.1×10^{-1}	5.0×10^{-2}	4.4×10^{-1}
10	2.2×10^{-4}	1.1×10^{-3}	5.4×10^{-3}	3.6×10^{-2}	2.8×10^{-2}
1	4.3×10^{-5}	1.6×10^{-3}	2.1×10^{-3}	3.7×10^{-2}	3.2×10^{-2}
0.1	6.7×10^{-5}	1.6×10^{-3}	1.6×10^{-3}	3.8×10^{-2}	2.9×10^{-2}

Table 3: Maximum absolute fitting error dependency on BPM resolution. Coefficients were normalized to 10σ. Tracked map was 9-th order.

must be sufficiently linear or its nonlinearity must be known and extracted. Otherwise, our measured data set will consist of the nonlinearity due to BPMs as well as beam dynamics. We will not discuss details about BPM nonlinearity, which should be negligible in well-calibrated BPMs[11, 19]. A novel beam based calibration procedure is under investigation. Note that BPM nonlinearity which is significantly above the BPM noise level will ruin map measurement and yield false information, while low BPM resolution will limit our ability to extract the information. Limitations will be revealed during data analysis.

The other concern is BPM resolution, which is often limited by its signal digitizer. Although such BPM data error often appears as uncertainty in the least-significant bit instead of being continuously distributed, we add uniformly or Gaussian distributed random errors to the data pairs generated with the LER map to simulate BPM resolution effects, since the least-squares fitting is not very sensitive to the error distribution. To fit the data (generated with a 9-th order map), we have used a 5-th order Taylor map (instead of 9-th order) in order to show that low order map can be used to fit high order maps as long as high order terms are weak.

Table-3 presents the simulation results with BPM resolutions of $100\mu m$, $10\mu m$, $1\mu m$, and $0.1\mu m$. We see that the possibility to extract nonlinear coefficients is dramatically improved from $100\mu m$ to $10\mu m$, while roughly constant for resolutions better than $10\mu m$. Comparing to Table-2 shows that below $10\mu m$, BPM errors are not significant and fitting errors (due to the low order fit-map used) dominate. Fig. 2 plots the fitting errors of each coefficient for the $10\,\mu m$ case, which is hoped for PEP-II. The coefficient indices are grouped by orders with boundaries at 5, 20, 55, 125, 251 for the 1st, 2nd, etc. orders respectively. It is exciting to realize that with $10\mu m$ BPM resolution, it is possible to measure the map to an unprecedent high order and accuracy. The data in Tables 2 and 3 demonstrate that map measurements should be capable of measuring significant nonlinearities, which is very important for accelerator diagnosis.

Although present technology is able to reach $10\mu m$ (if not much better) BPM resolution, few machines can offer such turn-by-turn resolution at this moment because the technology is relatively new and budget is always a concern. Therefore, for the time being, BPM resolution is the major obstacle for map measurements. We are exploring the possibility to use multiple BPMs simultaneously in order to gain some statistical benefit in phase space measurements.

In addition to BPM resolutions, energy resolution is also important. We assumed no δ

δ res.	orders				
	1-st	2-nd	3-rd	4-th	5-th
6×10^{-6}	1.8×10^{-4}	2.2×10^{-3}	4.9×10^{-3}	3.8×10^{-2}	5.1×10^{-2}
6×10^{-5}	4.9×10^{-4}	1.6×10^{-3}	5.7×10^{-3}	3.0×10^{-2}	3.8×10^{-2}
3×10^{-4}	9.4×10^{-4}	8.8×10^{-3}	3.0×10^{-3}	4.6×10^{-2}	2.1×10^{-1}
6×10^{-4}	3.7×10^{-3}	2.1×10^{-3}	1.0×10^{-1}	3.9×10^{-2}	5.3×10^{-1}

Table 4: Maximum absolute fitting error dependency on beam energy resolution.

errors in Table-3. Dependency on beam energy resolution for the $10\mu m$ case is tabulated in Table-4. In order to simulate the measurements, we used 15 equally spaced grid points (instead of random sampling) to cover the $\pm 4\sigma_\delta$ range. Table-4 shows that, to be consistent with the $10\mu m$ BPM resolution, we need energy resolution on the order of 5×10^{-5}. This corresponds to a signal-to-noise ratio of 50, which is much less than the requirement for transverse measurement. This is because we have to extract nonlinear motion out of fairly linear betatron oscillation transversely, while the linear and nonlinear dependencies on beam energy are comparable (the LER map we are using originates in a low dispersion region). Usually it is difficult to measure the beam energy accurately. Methods using a depolarizing resonance[29] or synchrotron radiation[30] are sufficiently accurate, but need special instruments. A method based on BPM measurements at high dispersion points[31] may be able to measure the relative energy change, but special care is needed in order to reach the required resolution. Typically omitted factors such as nonlinear dispersion coefficients may become significant. For our LER example, the dispersion function reads $\eta_1(1 - 1.9 \times 10^2\delta - 2.4 \times 10^4\delta^2 + 6.5 \times 10^5\delta^3 + 7.1 \times 10^8\delta^4 + \cdots)$ and $4\sigma_\delta$ gives $\delta_{max} \simeq 3 \times 10^{-3}$, which could yield up to 60% error (here the nonlinear effect is exaggerated by the low linear dispersion) when using only the leading term.

Instead of measuring the beam energy, Eq.(3) provides a way to change the beam energy accurately. When the RF frequency changed, the beam energy is forced to change according to Eq.(3) due to phase stability (assuming significant synchrotron oscillations are fully damped by radiation damping). The relative RF frequency change is better than 10^{-9}, and smooth approximation gives $\alpha_c \simeq \nu^{-2} \simeq 10^{-3}$, thus the accuracy of energy change depends on the linear and nonlinear momentum compaction factors. In general, the nonlinear momentum compaction factors are very weak. For LER we have $\alpha_c(1 + 1.6\delta - 45\delta^2 + 1.4 \times 10^3\delta^3 + 7.1 \times 10^5\delta^4 - 3.2 \times 10^7\delta^5 - 3.1 \times 10^9\delta^6 + \cdots)$. Therefore, we can drop the nonlinear part and still get fairly good resolution. However, we have to know the linear momentum compaction factor α_c to get the energy change correctly. To get a signal-to-noise ratio of 50, error in α_c should be less than 2%. Unfortunately, we may not know α_c sufficiently well and this may result in significant errors in the map coefficients. Nonetheless, notice that α_c is a scaling constant for the δ dimension, we still can get useful nonlinear information even though we do not know α_c exactly.

One more subtlety on beam energy is the calibration of the nominal energy. In order to compare with the design map, an absolute energy measurement is required. On the other

hand, lattice magnetic field errors may dominate the difference between the design and measured maps.[‖] Therefore it may not be necessary to know the beam energy better than $\Delta B_{err}/B$. However, better energy calibration will help to resolve lattice (closed orbit) errors with measured maps at various locations. Note that since the closed orbits are changing with beam energy, one must use the closed orbit at the nominal energy as a reference for all BPM readings. Also, for very high accuracy measurement, the energy difference around the ring due to synchrotron radiation may need to be taken into account, which is on the order of 10^{-4} and could result in 10^{-2} errors at 5-th order coefficients.

Before moving on to the next section, we present the exact (in diamond) and fitted (in dot) map coefficients in Fig. 3, which is the case of 10μm BPM resolution and 6×10^{-5} energy resolution. Except for the large leading linear coefficient (which is well fit), all coefficients up to 5-th order are shown in the figure. It shows that the map fitting method is very impressive in its potential of extracting nonlinear coefficients. We will discuss the errors in the following.

8 Error estimate and hypothesis test

For any measurement, it is important to obtain error estimates for the results. Besides factors affecting the existence and stability of the single-particle map, errors are mainly due to the BPM resolution and our hypothesis on the map order in the fitting procedure. BPM errors show up in the vector $\vec{x^f}$ and matrix A of Eq.(5). Errors in $\vec{x^f}$ are typical in least-squares fitting problems, whose effect can be estimated by the variance-covariance matrix [8]

$$\frac{\tilde{V}V}{m-n}(\tilde{A}A)^{-1} \tag{16}$$

where vector $V = \vec{x^f} - A\,\hat{C}$ (see Eq.5) and $\tilde{V}$ is its transpose. Square roots of the diagonal elements of the covariance matrix yield estimated rms errors of map coefficients, which are shown in Fig. 3 as error bars. Due to various reasons (eg. badly conditioned matrix A, measurement errors in A, relatively low fit-map order), the error bars given by Eq.(16) are not very good. A more reliable error estimate is under investigation. The factor $\hat{\sigma}^2 \equiv \tilde{V}V/(m-n)$ gives an unbiased estimate of the rms errors $\hat{\sigma}$ in measurement of $\vec{x^f}$, i.e. the BPM resolution, if the design matrix A is accurate. In our case, this is not exactly true. However, significant error bars for all coefficients will indicate problems due to BPM resolution.

In general, this kind of error can be reduced statistically with the usual $\frac{1}{\sqrt{m}}$ dependency by increasing the number of data pairs m since the expectation value of $\tilde{A}A$ is proportional to m. However, due to the errors discussed below, the accuracy of map extraction does not depend on Eq.(16) any more for sufficiently large m. Therefore, increasing the data size may be helpful only to some limited extent. Simulations presented before use a data size which is 10 times the number of coefficients to fit. As an example, Table-5 shows the dependency

[‖] One experimental way to define the nominal beam energy is to find the energy at which the closed orbit is centered at all sextupoles in average. This can be done by measuring the chromatic tune shifts at various sextupole strengths.

$m/250$	orders				
	1-st	2-nd	3-rd	4-th	5-th
4	1.1×10^{-3}	3.1×10^{-3}	1.4×10^{-2}	2.8×10^{-2}	9.8×10^{-2}
16	5.3×10^{-4}	1.9×10^{-3}	7.7×10^{-3}	2.9×10^{-2}	5.6×10^{-2}
64	1.3×10^{-4}	2.7×10^{-3}	2.6×10^{-3}	2.9×10^{-2}	2.1×10^{-2}
256	9.1×10^{-5}	1.7×10^{-3}	1.7×10^{-3}	3.0×10^{-2}	2.7×10^{-2}

Table 5: Maximum absolute fitting error dependency on number of data pairs. The 5-th order fit map has 250 terms.

on m for the case of $10\mu m$ BPM resolution and a 5-th order fit map. The first column lists m/n, i.e. the number of data pairs in units of the number of coefficients to fit.

The rms error estimate $\hat{\sigma}$ has another important application in our case. Since we measure a large number of data pairs over a period of time, it is possible to have some very bad data due to accidental events. Such data could significantly reduce fitting accuracy. One way to filter out such data is to check the fitting error of each data pair against $\hat{\sigma}$, and throw away data with an unreasonably large error. After such filtering, fit the map again as necessary.

Errors in matrix A are more complicated to evaluate because BPM errors show up non-linearly and their effects are map dependent. Using a perturbative approach, we can improve the estimate of Eq.(16) by adding

$$-2\,\hat{\sigma}^2 A^+ \,\mathrm{diag}[A_x \hat{C}]\,\check{(A^+)} \;+\; A^+ \sum_{\xi=\{x,P_x,\cdots\}} \hat{\sigma}_\xi^2 \,\mathrm{diag}[(A_\xi \hat{C})^2]\,\check{(A^+)} \tag{17}$$

where A_ξ characterizes the linear dependence of A on errors in ξ and can be computed from measured data. However, we will not go into the technical details of Eq.(17) here. Another possible, although primitive, way to improve the error estimate is to choose many (may overlap) subsets of the original data set, and obtain different fittings of the coefficients, which indicate the possible error bar. In this way we get a rough estimate of the maximum fitting errors for the $10\mu m$ BPM resolution and 6×10^{-5} energy resolution case, which yield $3.9(\pm 2.3)\times 10^{-4}$, $1.6(\pm 0.6)\times 10^{-3}$, $8.3(\pm 5.7)\times 10^{-3}$, $3.7(\pm 0.4)\times 10^{-2}$, and $4.8(\pm 2.1)\times 10^{-2}$ for the 1-st to 5-th orders respectively. This method can also be used to check the consistency of the data. For example, the data collected at the beginning and end of the whole measurement may yield significantly different maps if there is slow (adiabatic) variation of the underlying map due to external perturbations.

Errors due to map order hypothesis have been shown in section 6. They are also map dependent and hard to estimate. Checking the convergence of different order fit maps is necessary. Another potentially very useful method is singular value decomposition (SVD). By checking the magnitudes of singular values, one may determine at which order the fitting is not sensitive to its coefficients anymore. One may attempt to use a statistical hypothesis test also. Note that the (quasi-) symplecticity of the map implies nonlinear constraints among the coefficients, which makes usual hypothesis test routines inappropriate. Rigorous statistical theory for error estimates and hypothesis tests in our case would be interesting but not essential to this paper.

In this paper, we treat the 5D phase space equally and simultaneously. It is possible to break down the problem into lower dimensions, especially for the δ degree of freedom since it is not changed by the map. The advantage is that the parameter space for fitting can be reduced by many fittings in subspaces instead of a single step fitting in 5D. This could be important since one may need to fit thousands (2000 for 9-th order) of coefficients, which requires handling huge matrices. It is actually more natural to work with 4+1 dimensions if synchrotron oscillation is negligible. However, it is not expected to be significantly different in terms of fitting results. Further studies are required to settle this issue. The possible drawback to break down dimensions is that it may not always be possible for the 4D transverse phase space due to existence of coupling. Moreover, the process to filter out subspaces is likely to be an additional error source for fitting due to unavoidable coupling, even though it may be very weak in well tuned machines.

9 Error reduction

To reduce the errors due to fitting, the first thought is impose symplecticity. Even if the underlying map is symplectic, since Taylor maps do not respect symplecticity, the fitted map will not be symplectic. Therefore one is attempted to throw away the worst-fit coefficients and use symplectic constraints among coefficients to compute them. However, straightforward methods seem not to help.

Readers experienced in least-squares fitting problems may have suspected that the problem we formulated in Eq.(5) is ill-conditioned. Indeed that is the case. In fact, we believe that fairly amount of fitting errors are due to very large condition number of the design matrix A. We are exploring better numerical algorithms such as column weighting, orthogonal factorization etc. to reduce the numerical errors given the ill-conditioned matrix A. Note that the huge and dense matrix A (on the order of 10^6 elements for a 5D, 5-th order fit-map) makes the problem more difficult due to computer memory limitation.

Another obvious avenue to explore is to improve fundamentally the condition of the design matrix A by formulating the fitting problem in a series based on a properly chosen orthogonal basis. Due to the orthogonality of the basis, there are many advantages to work with them (eg. calculation of A^+ is simple and no numerical errors involved; the least-squares solution gives the generalized Fourier coefficients). Unfortunately, for our multi-variable problem, it is not trivial to take advantage of an orthogonal basis. It is even harder to choose the right series to improve the condition number of A. However, it is surely worthwhile to explore possibilities.

The other issue that concerns the fitting method is finding the optimal pattern (initial conditions) to sample the phase space. Results presented in this report are based on random sampling excluding the neighborhood of origin. A few other sampling patterns, such as uniform grid, were explored but no significant improvement has been achieved. This question is closely related to dimension and choice of expansion basis. It is probably necessary to break down the 5D problem and/or to use an orthogonal basis to take advantage of sampling patterns.

10 Conclusion

We analyzed the possibility to measure the Poincaré section map of a circular accelerator in normal operation mode. Our results show that presently available beam position monitors allow one to extract map coefficients with exciting high order and accuracy. If confirmed with experiments, such measurements could have a positive impact on accelerator physics studies. Although our analyses in this paper are based on the PEP-II low energy ring, the results are generic. Simulations for SPEAR and PEP-II high energy ring have also been done and results are similar.

Various issues concerning map measurements are addressed. The fundamental limit to the measurements are the physical existence of a stable single-particle map. Practically, BPM accuracy imposes certain limit, which is the major one for the time being. If BPMs are specially designed for very low current and high accuracy (for electron rings, $10\sigma_x \frac{\tau_0}{\tau_x}$ is about the best resolution one may need), the stability of the single-particle map in face of various external disturbances will set the final limit to the map measurements. Due to primitive nature of our method, it is hard to imagine other methods may work if our method fails to extract the nonlinearity of an accelerator due to BPM resolution or wake fields.

There are already a few accelerators (e.g. electron ring SPEAR and proton ring IUCF) capable of tracking beam phase space positions turn by turn. Experimental studies will be pursued as soon as possible to confirm our finding and identify possible unexpected problems.

11 Acknowledgement

The author C. X. Wang would like to acknowledge many helpful discussions with A. Chao, Y. T. Yan, M. Lee, J. Sebek, W. J. Corbett, G. V. Stupakov, and S. Heifets. Special thanks are due to A. Chao for reading and commenting the manuscript, and to Y. T. Yan for providing the one-turn map of PEP-II. This work is supported by the Department of Energy under contract DE-AC03-76SF00515 and the Applied Physics Department of Stanford University.

References

[1] W. J. Corbett, et al., Proc. of PAC 1993, p.108

[2] T. Barklow, et at., SLAC report PUB-5695

[3] P. Tran, et al., Proceedings of the 1995 Particle Accelerator Conference, p.3323

[4] A. W. Chao, et al., Phys. Rev. Lett., v.61, no.24, p.2752, (1988)

[5] S. Y. Lee, et al., Phys. Rev. Lett., v.67, no.27, p.3768 (1991)

[6] T. Chen, et al., Phys. Rev. Lett., v.68, no.1, p.33 (1991)

[7] G. A. Decker, AIP Conf. Proc. no.249, p.637(1991)

[8] W. C. Hamilton, Statistics in Physical Science, The Ronald Press Company 1964

[9] C. L. Lawson and R. J. Hanson, Solving Least Squares Problems, Prentice-Hall, Inc. 1974

[10] V. Balakin, EPAC94. Forth European Part. Acc. Conf., p.1539 (1994)

[11] G. R. Aiello and M. R. Mills, AIP Conf. Proc. no.281, p.301(1992)

[12] PEP-II An Asymmetric B Factory Conceptual Design Report, SLAC-418

[13] S. Heifets, et al., SLAC/AP-99 (1995)

[14] C. X. Wang and J. Irwin, Proc. of 1997 Part. Acc. Conf. p.??? (1997)

[15] I. C. HSU, Particle Accelerator, 1990, v.34, p.43

[16] R. E. Meller, et al., SSC report SSC-N360(1987)

[17] C. X. Wang and J. Irwin, AIP Conf. Proc. no.405 (1996)

[18] A. W. Chao, Physics of Collective Beam Instabilities in High Energy Accelerators, John Wiley & Sons Inc. 1993

[19] R. E. Shafer, AIP Conf. Proc. no.249, p.601(1991)

[20] M. Sands, "the Physics of Electron Storage Rings", SLAC report-121, 1970.

[21] P. Burla, et al., AIP Conf. Proc. no.326, p.167(1992)

[22] O. S. Bruning, et at., Phys. Rev. Lett., v.76, no.20, p.3719

[23] T. Katsura, et al., EPAC92. Third European Part. Acc. Conf., p.1631 (1992)

[24] L. Arnaudon, et al., Nucl. Instrum. Meth. A357, p.249(1995)

[25] Y. T. Yan, et al., Proceedings of the 1995 Particle Accelerator Conference, p.2765 (1995)

[26] Y. T. Yan, in Physics of Particle Accelerators, AIP Conf. Proc. no.249, p.380(1992) chapter 4

[27] Y. Cai, at al., Proceedings of the 1995 Particle Accelerator Conference, p.576 (1995)

[28] F. S. Acton, Numerical Methods that work, p.253, Mathematical Association of America 1990

[29] L. Arnaudon, et al., Phys. Lett. B 284, no.3-4, p.431(1992)

[30] I. P. Karabekov, Nucl. Instr. Meth. in Phys. Res. A 321, no.1-2, p.18(1992)

[31] S. Y. Lee, AIP Conf. Proc. no.326, p.18(1992)

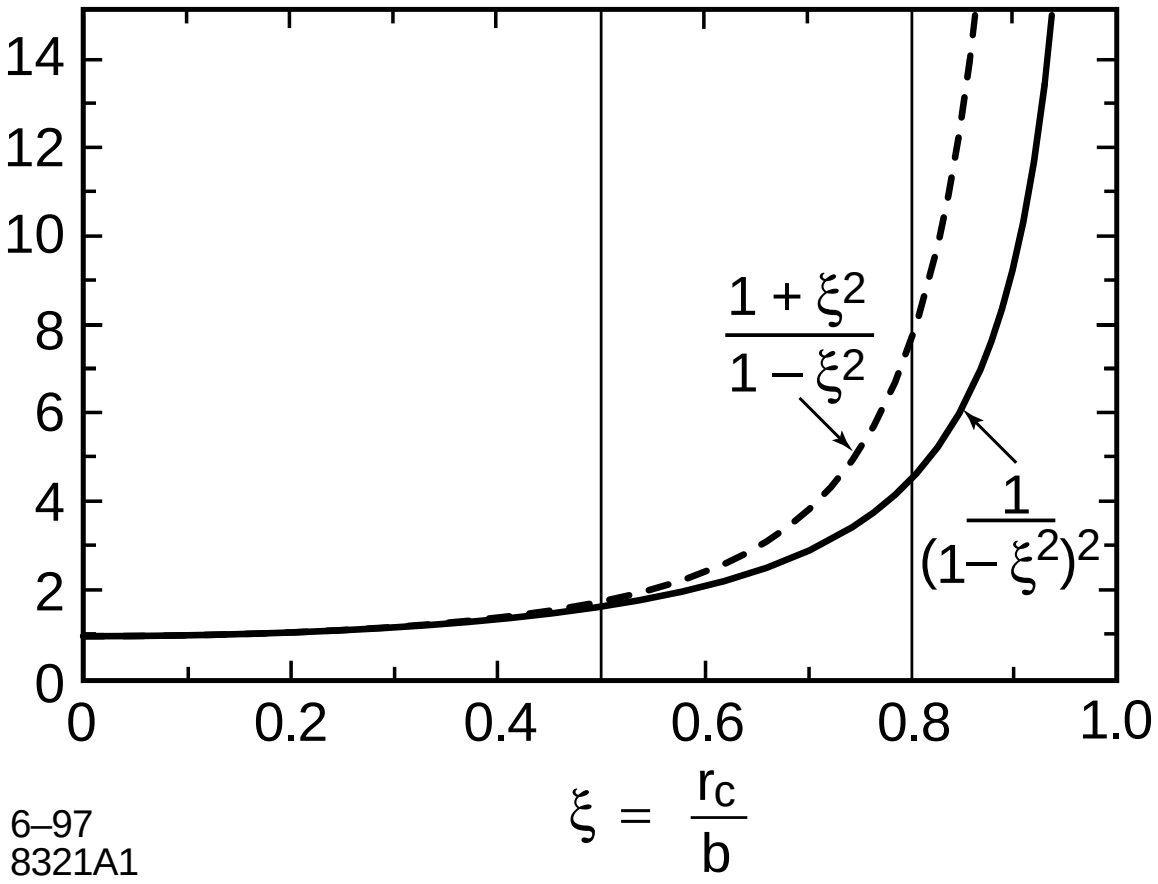

Figure 1: Nonlinear factors in the longitudinal and transverse (dashed) wake kicks

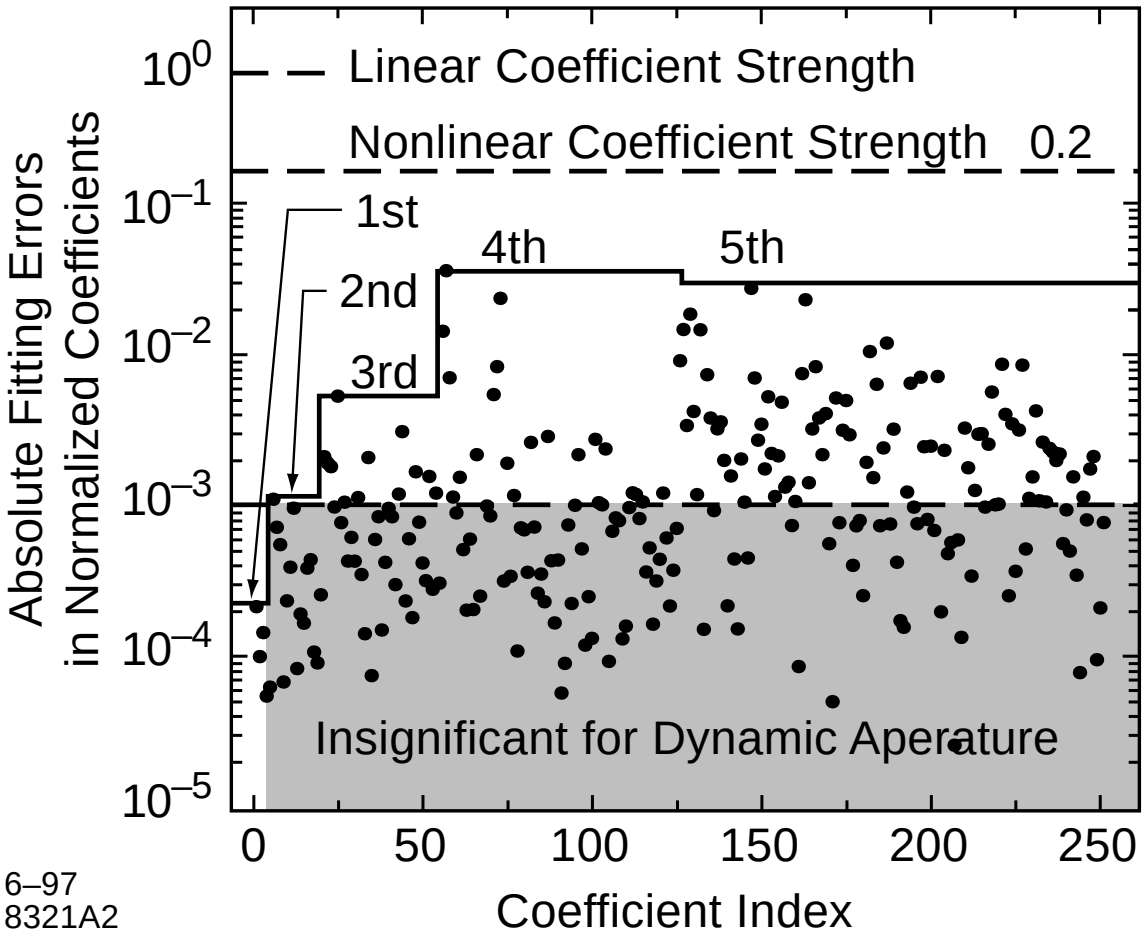

Figure 2: Absolute fitting errors for 10σ normalized map coefficients up to 5-th order

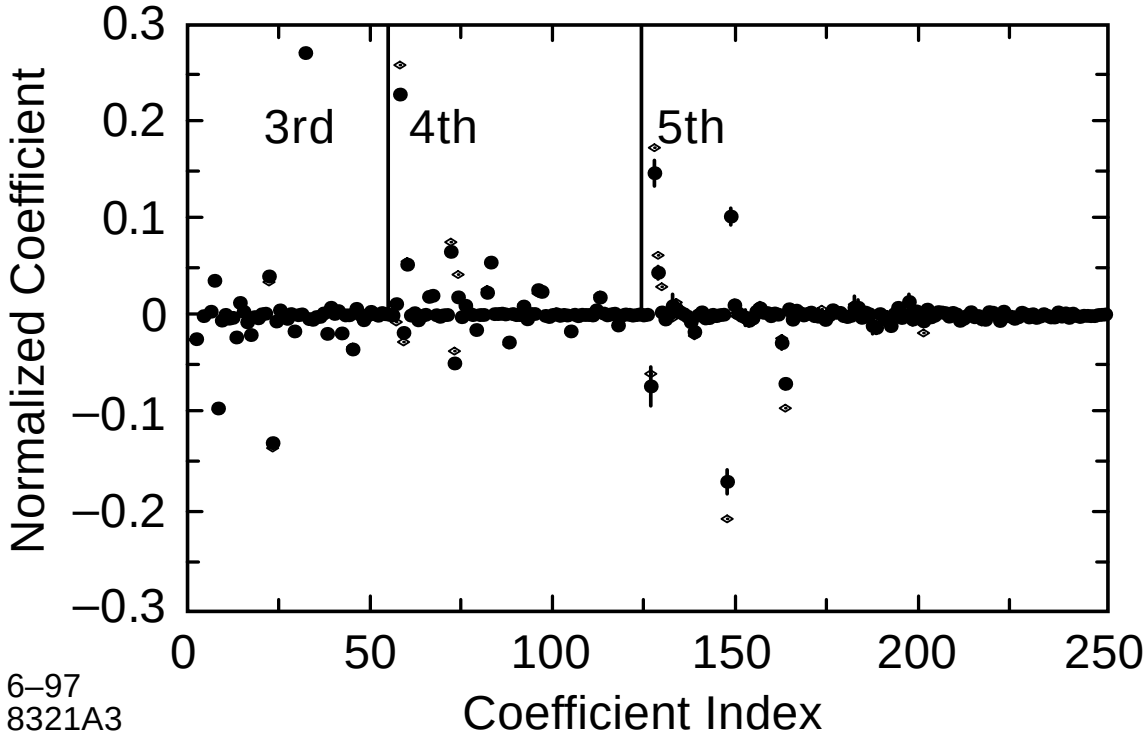

Figure 3: Comparison between exact (⋄) and fitted (•) map coefficients